



Article

# Recent Advances on the VAN Method

Nicholas V. Sarlis \*D, Efthimios S. Skordas D and Panayiotis A. Varotsos

Section of Condensed Matter Physics and Solid Earth Physics Institute, Department of Physics, National and Kapodistrian University of Athens, Panepistimiopolis, Zografos, 15784 Athens, Greece; eskordas@phys.uoa.gr (E.S.S.); pvaro@otenet.gr (P.A.V.)

\* Correspondence: nsarlis@phys.uoa.gr

#### **Abstract**

In the 1980s, Varotsos, Alexopoulos and Nomicos (VAN) introduced a short -term earth-quake (EQ) prediction method based on measurements of the electric field of the Earth at various locations on the Earth's surface. The corresponding electric signals are called Seismic Electric Signals (SES). Here, we present the advances of the VAN method during the period 2022–2025. For this purpose, we make use of the VAN telemetric network comprising of eight geoelectric field stations that have operated in Greece since the 1990s. The SES reported and documented well in advance (at arxiv.org) are compared with the subsequent seismicity in Greece during the same study period. The comparison reveals that all strong EQs of magnitude  $M \geq 5.8$  within the area  $N_{34.5}^{41.5}E_{20.0}^{27.5}$  have been preceded by SES activities, thus leading to a hit rate of 100%. The study of the present results points to the need of continuing VAN experimentation in Greece. Moreover, we employ the Receiver Operation Characteristics (ROC) method to evaluate the performance of the method. Study of the ROC reveals a false alarm rate of approximately 5% which is shown to be statistically significant, while the method can be characterized as outstanding.

**Keywords:** earthquakes; seismic electric signals; SES; VAN method; earthquake prediction; Greece



Academic Editor: Roberto Scarpa

Received: 1 September 2025 Revised: 22 September 2025 Accepted: 25 September 2025 Published: 28 September 2025

Citation: Sarlis, N.V.; Skordas, E.S.; Varotsos, P.A. Recent Advances on the VAN Method. *Appl. Sci.* **2025**, *15*, 10516. https://doi.org/10.3390/ app151910516

Copyright: © 2025 by the authors. Licensee MDPI, Basel, Switzerland. This article is an open access article distributed under the terms and conditions of the Creative Commons Attribution (CC BY) license (https://creativecommons.org/licenses/by/4.0/).

### 1. Introduction

Earthquake (EQ) prediction is the holy grail of seismology and many efforts have been devoted to this purpose, see, e.g., Refs. [1–46]. These efforts include ground measurements of the electric [1,3,5,6,9,14,22,32] and magnetic [4,14,17,23,27,28] field of the Earth, radon emissions [8,15], ionospheric perturbations [24,29,36,37], thermal anomalies close to the future EQ epicenter, see, e.g., [18], the lithosphere, atmosphere and ionosphere coupling [20,21] that allows the use of satellites [31] for EQ prediction purposes, changes in the level and temperature of confined groundwater [26], Earth's surface displacement [25], monitoring of seismic regimes [33,34,43,44] and deformation patterns [35,40,45,46], anomalies in borehole strain data [41], and measurable changes in seismicity, see, e.g., Refs. [38,39].

Varotsos et al. [47,48] introduced in the 1980s the so-called Varotsos-Alexopoulos-Nomicos (VAN) method of EQ prediction. This method is based on the measurement of transient changes in the electric field of the Earth called Seismic Electric Signals (SES) [5,49,50]. Several physical mechanisms have been proposed for the generation of SES, see, e.g., Figure 1.20 of Varotsos et al. [51], including the pressure-stimulated polarization currents (PSPC) emitted at the hypocenter suggested by Varotsos and Alexopoulos [52], see also [49]. SES are detectable at certain sites of the Earth's surface [49,53,54]. After extensive experimentation [5,49] in Greece since the 1980s, several SES sensitive sites have been selected

where dipoles were deployed for the measurement of the geoelectric field, see Figure 1. The data are collected via a telemetric network to the central station located at Glyfada, Athens. Further details on the telemetric network will be given in Section 2.2.

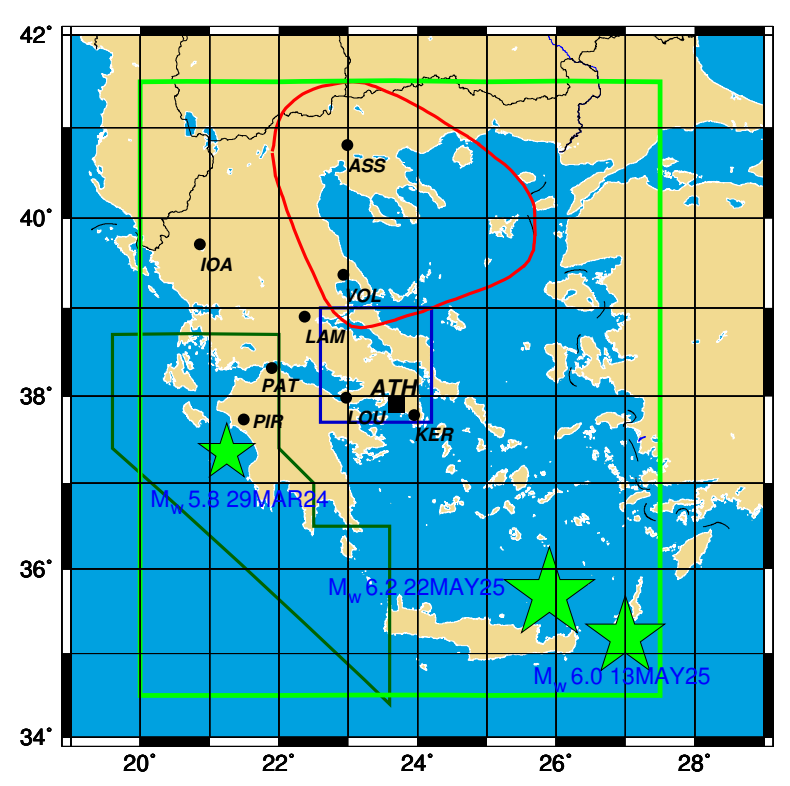


**Figure 1.** Map of Greece depicting the 8 geoelectric field stations with black circles: Assiros (ASS), Ioannina (IOA), Volos (VOL), Lamia (LAM), Patras (PAT), Loutraki (LOU), Keratea (KER), and Pirgos (PIR) of the VAN telemetric network. The central station at Glyfada, Athens (ATH), where data from the 8 field stations are collected, is shown by a black square. The green stars correspond to the epicenters of the EQs of magnitude  $M_{\rm w}>5.5$  reported—during the period 2022–2025—by the United States Geological Survey (USGS) [55] within the green rectangle that surrounds the area  $N_{34.5}^{41.5}E_{20.0}^{27.5}$ . The magnitude and date of occurrence are also shown for each EQ. The selectivity maps for PIR (dark green polygon), KER (blue rectangle), and ASS (red rounded triangle) are also shown.

Since 2001, the VAN method has led to many successful EQ predictions of strong EQs of magnitude  $M \geq 6.0$  in Greece, see Table 7.1 on page 296 of Varotsos et al. [51]. These include the 2008 magnitude [56,57]  $M_w6.9$  EQ [58], see, e.g., [59–61], which is the strongest EQ in southern Greece [62] since 17 January 1983  $M_w7.0$  EQ off shore Lixouri Kefalonia, Greece [63]. For earlier periods, the predictions issued can be found in Chapter 4 of Varotsos [50]. The statistical significance of VAN method predictions during the period from 1 April 1987 to 30 November 1989 has been recently studied[64] leading to p-values smaller or equal to 2% to obtain such results by chance. Since November 1995 [50,51], after the recommendation of the European Advisory Committee for EQ prediction of the Council of Europe, if the expected EQ magnitude M estimated from SES (see Section 2.1) is larger than or equal to 6.0, a quick report on the SES information is submitted to international journals or freely open preprint servers.

It is the purpose of the present paper to evaluate the performance of the VAN method during the recent almost 4-year period from 1 January 2022 to 31 August 2025 focusing on strong EQs having  $M_{\rm W} > 5.5$  as reported by USGS [62]. This allows for a plausible error  $\Delta M < 0.5$  in the estimation of the expected EQ magnitude [65]. The SES reported during this period are tabulated in Table 1 and labeled according to the VAN geoelectric field station at which they were recorded, see the fourth column of this Table. Among the new

Appl. Sci. 2025, 15, 10516 3 of 18

results obtained is a hit rate that may reach 100% with a false alarm rate of approximately 5%, which lead to the statistical significance (p=0.9%) of the method, which can be characterized as outstanding. Additionally, these last 4 years of seismic data can be used for improving the accuracy of the predictions since they provide details on the sensitivity of the VAN geoelectric field stations.

**Table 1.** List of the reported [66,67] SES. The first column corresponds to the date that the SES was recorded, the second column to the geoelectric field station that recorded the SES, and the third column provides a brief description of the related seismic activity. In the last column, the label used in this work for each SES is provided.

Date of SES	Station Name	Related seismic activity	Label
8 January 2023 <sup>1</sup>	ASS	$ m M_w 4.9$ on 7 February 2023 $^2$	ASS1
13 October 2023 <sup>3</sup>	PIR	M <sub>w</sub> 5.8 on 29 March 2024	PIR1
30 May 2024 <sup>1</sup>	KER	Drastic increase of ML(ATH)≥ 4.5 EQs	KER1
6 July 2024 <sup>3</sup>	PIR	$ m M_w 5.3$ on 21 July 2024 $^4$	PIR2
20 April 2025 <sup>1</sup>	KER	M <sub>w</sub> 6.0 and 6.2 on 13 and 22 May 2025	KER2

<sup>&</sup>lt;sup>1</sup> See Ref. [66]. <sup>2</sup> See Ref. [68]. <sup>3</sup> See Ref. [67]. <sup>4</sup> See Ref. [69].

The paper is organized as follows. In Section 2, we briefly review the methods used in the present research, the results are presented in Section 3 and discussed in Section 4. Finally, our conclusions follow in Section 5.

#### 2. Materials and Methods

Here, we briefly present the VAN method of EQ prediction, the VAN telemetric network operating now in Greece, give a short introduction to the Receiver Operating Characteristics (ROC) method used for the evaluation of the method and to provide information on the proposed physical mechanisms for SES generation.

### 2.1. Brief Description of the VAN Method

SES are low frequency  $f(\le 1 \text{ Hz})$ , variations of the electric field of the Earth that precede EQs. The duration of SES may vary from tens of seconds up to several hours or even more [5,70]. Various physical mechanisms have been suggested for SES generation, as will be further discussed in Section 2.4 below. Apart from their observations in Greece [50,51], SES have been observed in Japan [70–73], China [74–76], Mexico [77,78], and Kyrgyzstan [79]. It is interesting to note that for strong ( $M \ge 6.5$ ) EQs SES are accompanied by magnetic field variations, as a consequence of Maxwell's equations [14,80].

SES-sensitive sites, and hence the corresponding VAN geoelectric field station, collect SES from certain hypocentral areas, which are [53,54] either close to the station or connected through electrically conductive paths to the station. Hence, not all EQ epicenter location directions are equivalent as concerns a given VAN geoelectric field station. Moreover, it has been shown [81] that the ability of a station to measure SES is also related to the EQ mechanism. All these mean that for each VAN geoelectric field station, we can construct a map of the epicentral areas from which it can receive SES. Such a map is called [5] selectivity map, and its construction is based, of course, on past observations. The selectivity maps for the stations ASS, PIR, and KER mentioned in Table 1 are drawn in Figure 1.

In order to record SES, measuring electric dipoles of length L (of a few hundred meters up to several km) are deployed and the potential difference  $\Delta V$  is continuously monitored. Observations have shown that the most common case of SES comprises rectangular pulses of constant  $\Delta V$  deviation from the background similar to those shown in

Appl. Sci. 2025, 15, 10516 4 of 18

Figures 2b, 3, and 4. In such a case, the SES amplitude  $\Delta V/L$  is related to the expected magnitude M by the relation

$$\log_{10}(\Delta V/L) = (0.3 \text{ to } 0.4) \times M + b,$$
 (1)

where the constant b is different for each seismic area-dipole pair, this is the reason why the epicentral distance r is not involved explicitly, see Varotsos [50] for its physical explanation. Orihara et al. [73] replaced  $(\Delta V/L)$  by  $(\Delta V/L \times r)$  to allow for varying focal distances in the case of EQs generated close to the measuring dipole. The VAN method is based on the continuous observation and registration of SES that allows the application of Equation (1) for the estimation of M upon using existing data.

When deploying the measuring dipoles at VAN geoelectric field stations, see Section 2.2, various orientations are used so that the ratio of the SES amplitude along the East-West and the North-South directions  $(\Delta V/L)_{\rm EW}/(\Delta V/L)_{\rm NS}$  can be experimentally calculated. It can be shown[50] that this ratio is characteristic of the area probable to suffer the impending EQ. This way, by using previous experience, the future epicenter can be estimated.

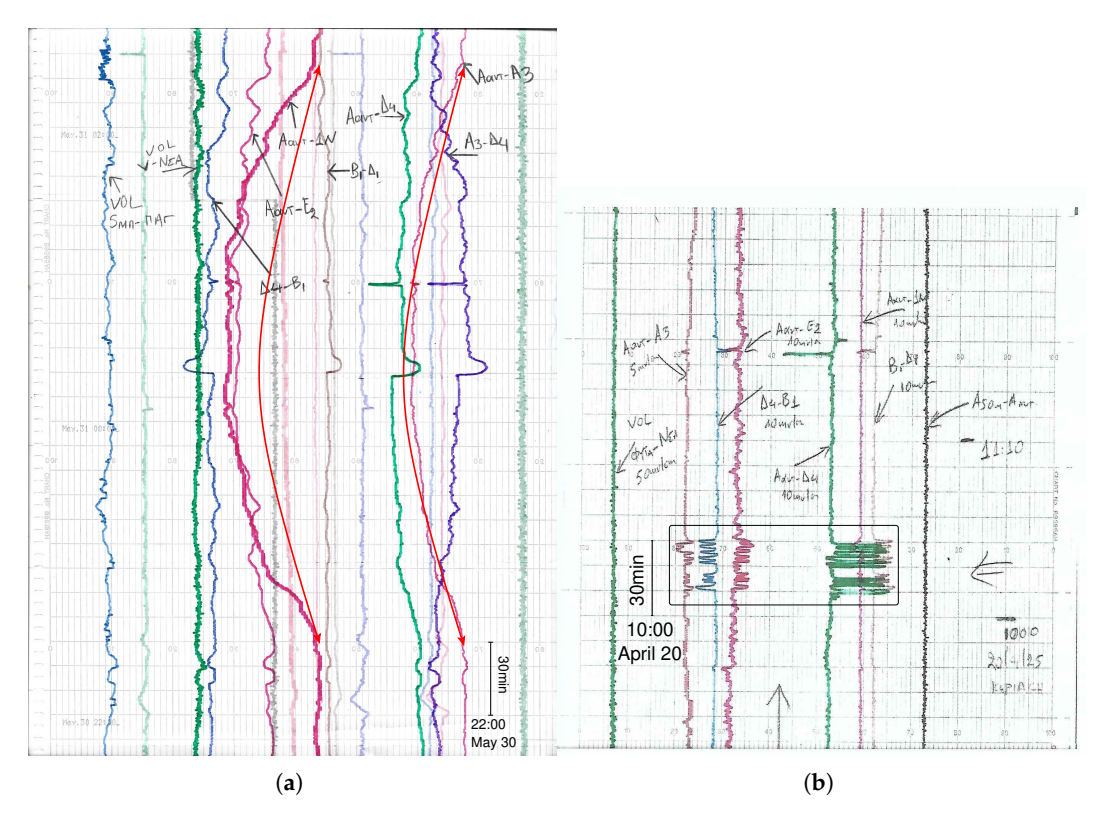
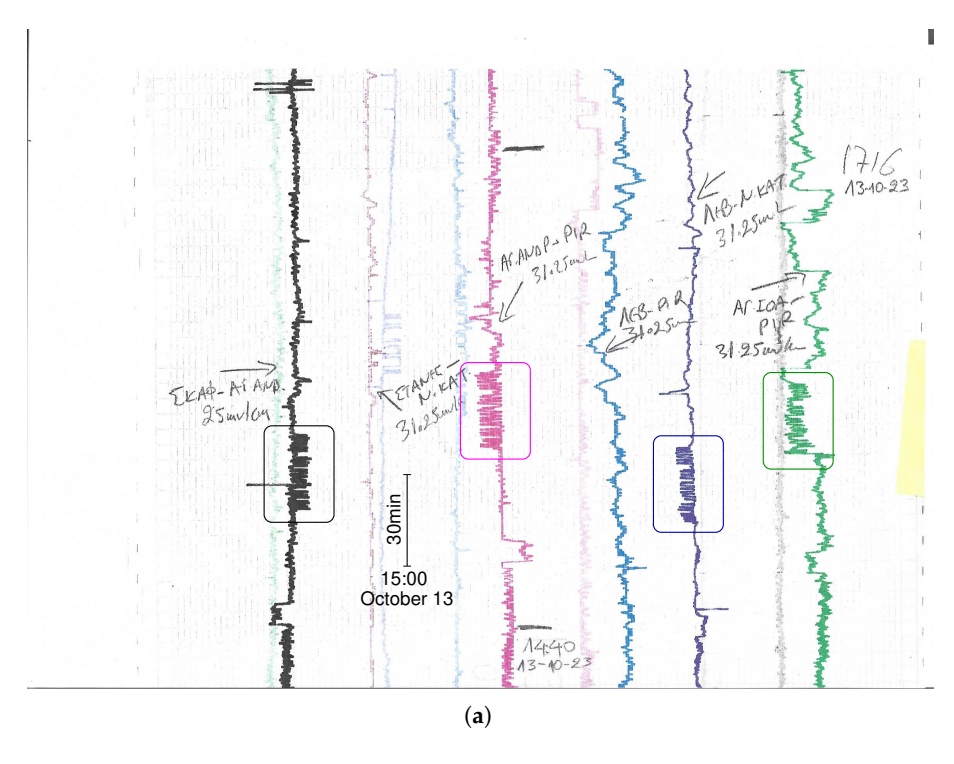


Figure 2. The SES recorded at KER geoelectric field station and reported before the corresponding EQ occurrences, see Table 1. (a) depicts SES KER1 which was recorded at channels  $A_{\alpha\nu\tau} - E_2$ ,  $A_{\alpha\nu\tau} - 1N$ ,  $A_{\alpha\nu\tau} - \Delta_4$ ,  $A_3 - \Delta_4$ ,  $A_{\alpha\nu\tau} - A_3$  of KER geoelectrical station from 22:30 UT on 30 May 2024 until 02:25 UT on 31 May 2024 having a characteristic *bay-like* shape. The two red arcs starting and ending with arrowheads indicate the duration and polarity of this *bay-like* variation (only channel  $A_3 - \Delta_4$  has opposite polarity exhibiting a deflection to the right). (b) corresponds to SES KER2 recorded on 20 April 2025, which is indicated by the black rectangle, with duration approximately 22 min. The SES maximum deflections from background are 45 mV (for channel  $A_{\alpha\nu\tau} - 1N$ ) and 35 mV (for channel  $A_{\alpha\nu\tau} - \Delta_4$ ) for KER1 and KER2, respectively.

Appl. Sci. **2025**, 15, 10516 5 of 18



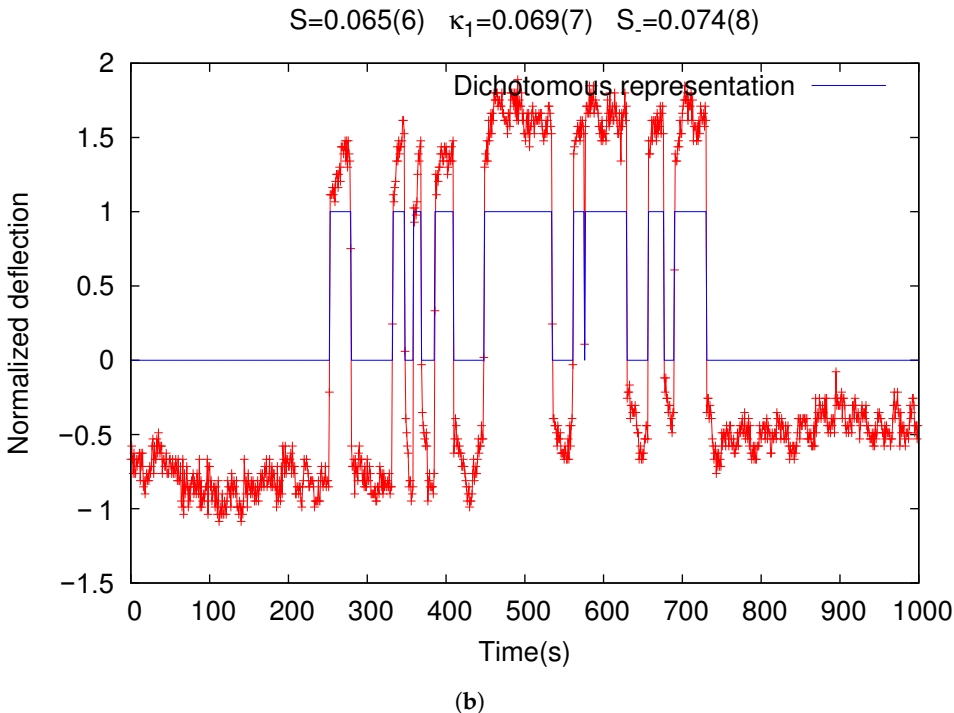
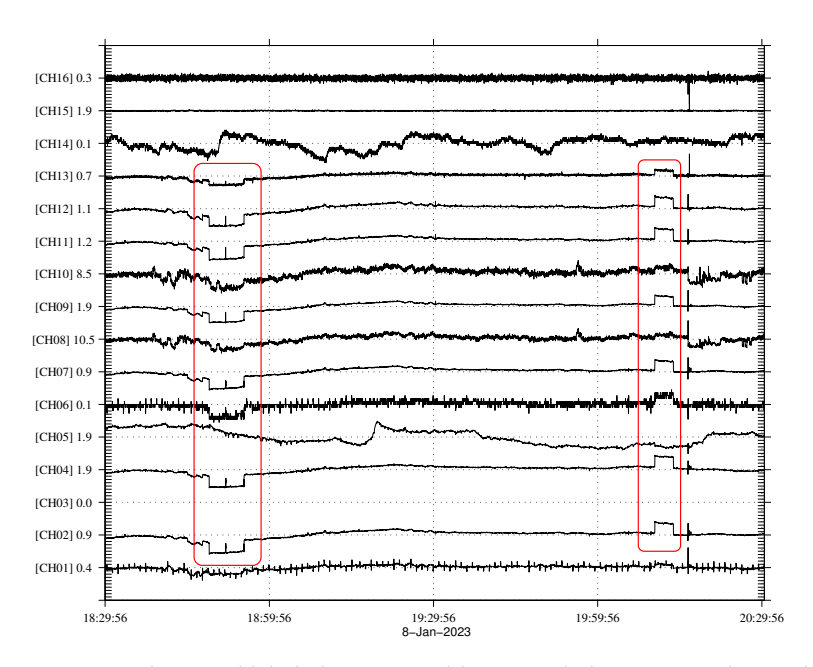


Figure 3. The SES recorded at the PIR geoelectric field station and reported before the corresponding EQ occurrences, see Table 1. (a) shows SES PIR1 using an excerpt of the raw data recordings at the central station of the telemetric network for the PIR station on 13 October 2023. Since data recordings from each measuring dipole are plotted with various delays to avoid overlapping, the simultaneous raw data at four measuring dipoles are surrounded by colored rectangles (of  $\approx$ 30 min duration) for the sake of readers' convenience. (b) illustrates SES PIR2 that was recorded at PIR on 6 July 2024. In this panel, the normalized deflection, i.e.,  $y = (\Delta V - \mu)/\sigma$ , where  $\mu$  and  $\sigma$  are the mean value and standard deviation of  $\Delta V$  during the interval shown, is plotted versus time elapsed from 11:40 UT. The SES maximum deflections from background are 10 mV and 6 mV for PIR1 and PIR2, respectively.

Appl. Sci. 2025, 15, 10516 6 of 18



**Figure 4.** The signal labeled ASS1 in Table 1 recorded at ASS geoelectrical field station on 8 January 2023. For the readers' convenience, it is enclosed by the red rectangles. The recordings of each measuring dipole are shown in varying vertical scales indicated by the numbers next to each channel (CH). The reported values are one-tenth of the peak-to-peak variation in mV.

The lead time of SES activities varies from a few weeks to  $5\frac{1}{2}$  months [51]. For simplicity, in the present paper we assume a maximum lead time of six months. This means that we consider as the period probable to suffer the impending strong EQ to be the first six months after the SES observation.

The discrimination of SES from man-made interference was traditionally [5,50] made by comparing the values of  $\Delta V/L$  between parallel measuring dipoles of different lengths L. If a (man-made) noise source lies between the electrodes of the two measuring dipoles, then the values of  $\Delta V/L$  differ significantly, see, e.g., Figure 21 of [49]. The fact that for SES  $\Delta V/L \approx {\rm const.}$  holds for parallel measuring electric dipoles is also compatible with the results obtained from theoretical models introduced to explain the selectivity effect [53,54]. After the introduction of Natural Time Analysis (NTA) in 2001 [13,51] the discrimination of SES from noise became possible even when using data from a single measuring dipole.

For this reason, we consider the representation of a SES in NTA: In the case of SES having rectangular shape as the one shown in Figure 3b, we define [13,51] the natural time for the occurrence of the k-th pulse by  $\chi_k = k/N$ . We then calculate the duration  $Q_k$  of each pulse  $k = 1, 2, 3, \ldots$  using the signal's dichotomous representation as shown by the blue line in Figure 3b. In NTA, we use the quantity  $p_k = Q_k/\sum_{n=1}^N Q_n$  as a normalized "energy" for the k-th pulse and study the behavior of the quantity [13,51]

$$\Pi(\omega) \equiv |\Phi(\omega)|^2 \tag{2}$$

defined by

$$\Phi(\omega) = \sum_{k=1}^{N} p_k \exp(i\omega \chi_k)$$
 (3)

where  $\omega$  stands for the angular frequency, for  $\omega$  close to zero. This way we capture the dynamic evolution of a complex system. This is so because  $p_k$  can be considered as probabilities and all moments of the distribution of  $p_k$  can be estimated from  $\Phi(\omega)$  at

Appl. Sci. 2025, 15, 10516 7 of 18

 $\omega \to 0$ , see p. 499 of Ref. [82]. To this purpose, the quantity  $\kappa_1$  is defined from the Taylor expansion  $\Pi(\omega) = 1 - \kappa_1 \omega^2 + \kappa_2 \omega^4 + \dots$  which equals:

$$\kappa_1 = \sum_{k=1}^N \left(\frac{k}{N}\right)^2 p_k - \left(\sum_{k=1}^N \frac{k}{N} p_k\right)^2. \tag{4}$$

As can be seen from Equation (4), the quantity  $\kappa_1$  is just the variance  $(\kappa_1 = \langle \chi^2 \rangle - \langle \chi \rangle^2)$  of natural time  $\chi$  with respect to the distribution  $p_k$ .

Apart from  $\kappa_1$ , another useful quantity in natural time is the entropy *S* given by [13]:

$$S = \langle \chi \ln \chi \rangle - \langle \chi \rangle \ln \langle \chi \rangle, \tag{5}$$

where the brackets  $\langle \dots \rangle \left( \equiv \sum_{k=1}^N \dots p_k \right)$  denote averages with respect to the distribution  $p_k$ . S is a dynamic entropy that exhibits [51] positivity, concavity, and Lesche [83,84] experimental stability. When  $Q_k$  are independent and identically-distributed random variables, S reaches [51] the value  $S_u \equiv \frac{\ln 2}{2} - \frac{1}{4} \approx 0.0966$  that corresponds to the "uniform" distribution. Upon reversing the time arrow and hence applying time reversal  $\mathcal{T}$ , i.e.,  $\mathcal{T}p_k = p_{N-k+1}$ , the value of S changes to a value  $S_-$ .

The study by NTA of various SES, see, e.g., Table 4.6 of [51], has shown that the following conditions are valid

$$\kappa_{1,\text{SES}} \approx 0.070,$$
(6)

$$S, S_{-} < S_{u} \tag{7}$$

### 2.2. Description of the VAN Telemetric Network

The VAN telemetric network was established in 1982 by the Greek scientists Varotsos, Alexopoulos, and Nomicos, and was named after their initials, as mentioned. Its purpose was the continuous measurements of the electric field of the Earth for the study of SES. This research was motivated by the detailed study of the thermodynamics of crystal defects in solids [50] that opened the possibility that rupture in solids could be preceded by transient electric signals. VAN telemetric network, consisting initially of eighteen measuring stations, was completed [85,86] by 1983 (see Figure 1 of [85]). The data were transmitted in real time [50,87,88] to the central station located in ATH. The dipoles, measuring the potential difference  $\Delta V$ , are consisting of non-polarizable electrodes  $Pb/PbCl_2$  and are submerged at a depth of 2 m. At least eight measuring electric dipoles of various lengths L and orientations were initially installed at each station, they are later optimized for SES detection and (man-made) noise discrimination by using  $\Delta V/L \approx \text{const.}$  criterion, see Section 2.1. Details of this procedure can be found in Section 2 of Varotsos et al. [49]. The dipoles of  $\sim$  50 m  $\leq L \leq \sim$  500 m are called short-dipoles, while the ones with  $\sim$  2 km  $\leq L \leq \sim$  20 km are called long-dipoles. During the 1990s, beyond the aforementioned real-time data collecting system, dataloggers (Campbell 21X connected to a portable PC) were installed at several stations to collect data with sampling rate  $f_s = 1$  sample/s. These data were initially stored only during SES collection, and during the period extending from several minutes before a significant EQ, until a few minutes after. Their average, 1 sample/20 s (cf. initially was 1 sample/10 s), were transmitted daily to the central station through dial-up. In 2010s, the dial-up collection was replaced by GSM and all data, either of a sampling rate of 1 sample/20 s or of  $f_s$  =1 sample/s are automatically transmitted to the central station daily.

# 2.3. Receiver Operating Characteristics

Receiver Operating Characteristics (ROC) [89] can be used for the evaluation of binary prediction methods. Assuming that there are P "strong" events to be predicted out of

Appl. Sci. 2025, 15, 10516 8 of 18

N(=P+Q) events, one defines as true positives (TP) the cases where a strong event is predicted and it actually occurs as true negatives (TN), the number of cases with no strong event is predicted, and it does not actually occur. Similarly, false positives (FP) are the cases when a strong event is predicted but it does not actually occur and false negative (FN) when a strong event occurs that was not predicted. ROC is a diagram of the hit rate, or true positive rate, which equals TP/P versus the false alarm rate, or false positive rate, which equals PP/Q = PP/(PP+TN). This way ROC takes into account the two sources of error in predictions, i.e., missing a strong event and providing a false alarm [89].

Upon varying the threshold used for the prediction of strong events, we get a curve on the ROC diagram. Random predictions correspond to the diagonal in the ROC diagram since on average they lead to the same values of the hit and alarm rates. However, when P and Q are small, e.g., N < 100, fluctuations around the diagonal occur.

The statistical significance of a prediction method is estimated by the area under the curve (AUC) in the ROC plane [90]. Mason and Graham [90] showed that AUC =  $1 - \frac{U}{PQ}$ , where U follows the Mann–Whitney U-statistics [91]. Using this result, the statistical significance can be visualized using k-ellipses which are envelopes of confidence ellipses centered along the diagonal [92,93]. Using the AUC of the k-ellipse that passes through a point in the ROC plane, we can obtain an estimate of the probability p (or p-value) to obtain by chance this ROC point [92]. Hence, we estimate the statistical significance of a prediction method, even if we can have a single point in the ROC plane.

Note that in medicine, AUC is a widely used to summarize the overall diagnostic accuracy of a test, e.g., see Ref. [94]. When AUC varies in the range 0.7 to 0.8 the test is considered acceptable, while when AUC lies in the range 0.8 to 0.9 it is characterized excellent, AUC more than 0.9 is outstanding [95]; see also Chapter 5 of Ref. [96].

## 2.4. Physical Mechanisms for the Generation of SES

As mentioned in the Introduction, a physical mechanism for the generation of SES is PSPC. PSPC are emitted upon increasing pressure (or stress) when the relaxation time of the dipoles formed due to aliovalent impurities in the ionic crystals which are constituents of rocks is minimized giving rise to a significant current that can be measured at appropriate sensitive sites on the Earth's surface [49–52]. Beyond the PSPC model introduced in 1980s by Varotsos et al. [47,48] to explain the precursory electric signals several other physical mechanisms have been suggested.

Examples are: First, electrokinetic phenomena can provide the basis for the generation of electrical precursors (e.g., see Refs. [97-106]) where the electric field results from fluid flow through the crust in the presence of an electric double layer of the solid-liquid interfaces (this fluid flow transports the ions in the fluid in the direction of flow, thus leading to electric currents). Second, around the focal area, considering EQ rupture as a critical point [107], e.g., coalescence of microfractures of foreshocks and/or fluctuations at the measuring sites. Third, Slifkin [108,109] suggested the charged dislocation mechanism for the generation of SES activities. According to this model, electric dipoles are produced upon abrupt stress variation in materials with significant concentrations of impurities, such as geophysically interesting materials such as silicates, oxides, and the like. In these materials, the space charge around an electrically charged edge dislocation consists largely of aliovalent ions. Fourth, the model of the large-scale motion of lattice defects introduced by Lazarus [110]. This is based on a phase transition associated with large-scale motion of lattice defects. This transition is confined to a thin region immediately adjacent to and parallel to the fault plane, e.g., from a hydrous to an unhydrous form of a mineral. Note that nearly all terrestrial minerals are formed with a varying amount of water crystallization in the lattice. Upon increasing stress, these minerals must transform to unhydrous phases expelling the water.

The compression of the lattice at this phase transition would cause large-scale (deformation and hence) motion of lattice defects, which would result in a large electrostatic signal generating the SES.

#### 3. Results

Here, we present the results related to the SES reported during the study period 1 January 2022 to 31 August 2025 which are shown in Table 1. They are presented below according to the VAN geoelectric field station at which they were recorded.

### 3.1. SES Recorded at KER Geoelectric Field Station

Two SES labeled KER1 and KER2 have been recorded at the KER geoelectric field station, and are shown in Figure 2.

SES KER1 was recorded on 30 May 2024 and reported as such on 5 June 2024, see Reference [61] of Varotsos et al. [66]. It lasted approximately 235 min from  $\approx$ 22:30 UT on 30 May 2024 until 02:25 UT on 31 May 2024, see Figure 2a. It has a characteristic *bay-like* shape and a significant duration of approximately four hours. SES of similar shape are very rare. Such a gradual variation of the geoelectric field is unlikely to be generated from PSPC but other physical mechanisms like the electrokinetic effect might be responsible for their generation [99], see also Section 2.4. For example, since the 1980s, the only reported case of a *bay-like* shape SES is the one recorded at KER during the period from 17:52 UT on 8 September 1986 until 05:50 UT on 9 September 1986, see Figure 1 of Varotsos and Alexopoulos [111]. It was followed by the 13 of September 1986 destructive  $M_w$ 6.0 EQ [112] that hit the city of Kalamata, Greece, killing 20 people [113].

Fortunately, KER1 was not immediately (within 6 months) followed by an M6 class EQ in Greece. However, instead of a single M6 class EQ a series of smaller EQs occurred in Greece. To study this phenomenon, we examine the smaller EQs measured by the Institute of Geodynamics of the National Observatory of Athens (GI-NOA), where the magnitude ML(ATH) is reported, that occurred within the area  $N_{34.5}^{39.5}E_{20.0}^{25.0}$  that mainly focuses on southern Greece taking also into consideration the northern (N39.0°) and western (E24.2°) edge of the KER selectivity map, see Figure 1. Using the EQ catalog[114] of GI-NOA, we find that for the period 1 January 2022 to 1 July 2024 the average number  $\lambda$  of EQs of magnitude ML(ATH)  $\geq 4.5$  per six months is  $\lambda = 4.6$  (Note that the last such EQ before 1 July 2024 occurred on 14 April 2024, i.e., before KER1 SES observation). Interestingly, after KER1 observation during the period 1 July 2024 to 31 December 2024 n = 10 EQs with  $ML(ATH) \ge 4.5$  have been observed. According to the Poisson distribution, this is highly unlikely since for  $\lambda = 4.6$  the probability to observe more than nine such EQs within six months is Prob(n > 9) = 1.95%. Additionally, when examining the first six months of 2025 we again find n = 10 EQs, meaning that after the KER1 observation a highly improbable EQ sequence occurred with a p-value  $p = 0.0195^2 = 3.8 \times 10^{-4}$ .

We now turn to SES KER2 shown in Figure 2b that was recorded on 20 April 2025 and reported on 25 April 2025 (see Reference [64] of Varotsos et al. [66]). Twenty-three days later the  $M_w6.0$  EQ shown in Figure 1 took place. This was followed after nine days by the  $M_w6.2$  EQ also shown in the same Figure. The lead time of 23 days falls within the periods identified [64] (see the third line of their Section 4) as statistically significant for SES precursors. The lead time coincidence together with the fact that up to date no other M6 class EQs occurred within the KER selectivity map, make us interrelate the two stronger EQs of Figure 1 to SES KER2. This association is in the same sense as the aforementioned 1986  $M_w6.0$  Kalamata EQ (at N37.0° E22.2°) was interrelated with the 1986 bay-like shape SES at KER. These connections emphasise the importance of the KER geoelectric field station on monitoring the seismic activity in southern Greece.

#### 3.2. SES Recorded at PIR Geoelectric Field Station

Two SES labeled PIR1 and PIR2 have been recorded at the PIR geoelectric field station, and are shown in Figure 3.

SES PIR1, of duration  $\approx$ 26 min, was recorded on 13 October 2023 and reported on 21 October 2023 (see Reference [92] of [67]). It was followed by an M6 class EQ, i.e., the  $M_w5.8$  EQ that occurred on 29 March 2024 within the selectivity map of the PIR station (shown in Figure 1 of [32]). The identification of PIR1 as SES was facilitated by employing NTA. The latter led to values S=0.066(3),  $\kappa_1=0.069(3)$ ,  $S_-=0.083(4)$  which are compatible with Equations (6) and (7).

On 6 July 2024, another SES labeled PIR2, see Figure 2b, with duration 6.4 min was recorded at the PIR station. It was reported on 13 July 2024 (see Reference [95] of [67]). NTA of PIR2 led to values S = 0.065(6),  $\kappa_1 = 0.069(7)$ ,  $S_- = 0.074(8)$ , which satisfy the conditions of Equations (6) and (7) for being considered as SES. PIR2 was not followed by an M6 class EQ but rather by the  $M_w5.3$  EQ that occurred two weeks later on 21 July 2024 with an epicenter at N34.9°E 23.2° inside the selectivity map of PIR.

#### 3.3. SES Recorded at ASS Geoelectric Field Station

On 8 January 2023 the signal shown in Figure 3 was recorded at ASS geoelectric field station and reported on 12 January 2023 (see Reference [54] of [66]). Signal ASS1 involves three rectangular pulses of duration between 3 and 3.5 min which are enclosed by the red rectangles in Figure 3. The first two pulses are adjacent (both included in the first rectangle), while the third one has a different polarity. Since various measuring dipoles are oriented in different directions, and depending on their good operation, not all channels record ASS1. The maximum deflection from the background is 9 mV. The strongest EQ that occurred within the selectivity map of ASS is an  $M_w4.9$  EQ on 7 February 2023 [68] with an epicenter at N40.2° E23.6° approximately 90 km southeast of ASS geoelectric field station.

#### 4. Discussion

First, we classify the five SES of Table 1 as either hits or false alarms. Considering that we focus on the prediction of magnitude 6 class EQs, the results presented in Section 3.2 show that SES PIR1 is a hit since it preceded by approximately  $5\frac{1}{2}$  months the  $M_w5.8$  EQ shown in Figure 1. On the other hand, SES PIR2 and ASS1 should be counted as false alarms since they were followed by EQs of significantly smaller magnitudes, see Table 1.

Moreover, SES KER1, which is of *bay-like* shape, and was followed by a significant and highly unlikely increase of the seismic activity without any strong ( $M_w > 5.5$ ) EQ should be also considered as a false alarm. SES KER1 convinces us about the necessity to continue the long-time experimentation based on the VAN telemetric network since it is the second time in almost 40 years that such a *bay-like* shape has been recorded. Recalling that the previous observation of such a SES [111] was followed by the 1986  $M_w$ 6.0 EQ close to the city of Kalamata [112], we consider that the KER station apart from recording SES close to its vicinity—as indicated in its selectivity map [115]—it provides precursory information for a wider area in southern Greece. In the future, both these *bay-like* shape SES could be used for EQ prediction. A fact that differentiates between these two SES is their duration, which is much larger in the case of the 1986 SES.

We now turn to the case of SES KER2, which was followed within a month by the two  $M_w6.0$  and 6.2 on 13 and 22 May 2025 EQs are shown in Figure 1. This case should be considered as a hit due to the immediate time correlation between the EQs and the SES. Further analysis of KER2 by NTA reveals that the corresponding values of S=0.065(5),  $\kappa_1=0.064(6)$ ,  $S_-=0.066(8)$  satisfy the conditions of Equations (6) and (7). Additionally, as mentioned in the previous paragraph KER station provides precursory information for a

wider area in southern Greece, thus, it is not unlikely that these two EQs to be related to KER2 although their epicenters lie outside the KER selectivity map[115].

We now separate our study period 1 January 2022 to 31 August 2025 into (approximately) 8 six-month periods. Since eight VAN stations, see Figure 1, could have recorded SES during this study period (cf. in the past all of them recorded electric signals related to EQs: Beyond the examples listed in Table 1, for IOA see [14], for VOL see [116], for LAM see [117], for LOU see [50], and for PAT see [118]) there are in total  $8 \times 8 = 64$  slots for which predictions could have been issued. According to the definitions of Section 2.3, this means that N = 64 with P=2 (since out of the 3 strong EQs of Figure 1 two of them occurred within ten days) and Q = 62. Summarizing the previous paragraphs, we have three false alarms, i.e., FP = 3, corresponding to SES ASS1, KER1, PIR2 and two hits (TP = 2) for SES PIR1 and KER2. These lead to the operation point with hit rate = 1 and false alarm rate = 3/62 = 4.8% shown by the red circle in the ROC diagram of Figure 5. Using k-ellipses [92,93], we estimate that such an operation point has a p-value to be obtained by chance equal to p = 0.9%. The AUC of the k-ellipse passing through this operating point is 0.99, which is characterized [95] outstanding. Even if we allow KER2 to be considered as a false alarm (negating the strong time correlation with the two strongest EQs in Figure 1), we obtain a hit rate of 50% and and false alarm rate = 4/62 = 6.5% leading to p = 2.5% and AUC = 0.91 which is still characterized [95] outstanding. Thus, the VAN method for both cases is statistically significant and can be characterized as outstanding.

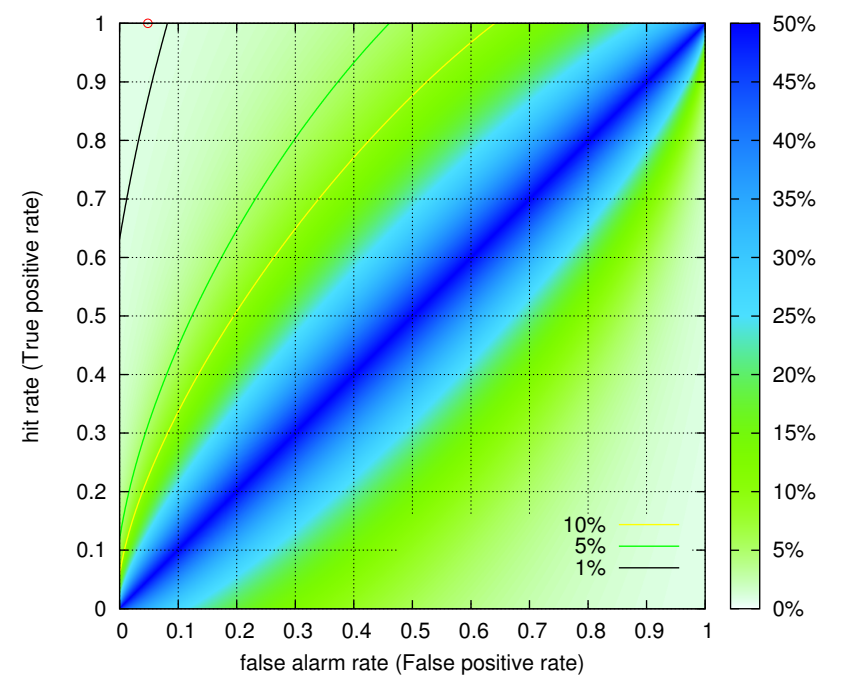


**Figure 5.** Receiver Operating Characteristics for the represented analysis of the application of the VAN method in Greece during the period 1 January 2022 to 31 August 2025. The operation point corresponds to the red circle in the upper left corner of the ROC and has p-value to be obtained by chance p = 0.9%. The color contours correspond to k-ellipses [92,93] with p-values indicated by the right colorbar.

Comparing the results of Figure 5 with those of Figure 4 of [64] —which corresponds to the analysis of SES predictions from 1 April 1987 to 30 November 1989 in Greece—having a hit rate  $\approx 0.3$  and false alarm rate  $\approx 15\%$ , we observe a significant improvement during the present study period. This is certainly related to the improvement of the VAN telemetric network, the fact that since 1995, SES are reported only when the expected magnitude M is equal to or larger than 6.0 as well as the introduction [13,39,51] of NTA in 2001. At this

point we have to comment that in the case of ASS1 of Figure 4 NTA could not be applied because it consists of only three pulses. This might be the reason behind that ASS1 is a false alarm.

As concerns the importance of reporting SES only when the expected magnitude M is equal to or larger than 6.0, we have to mention that if we consider EQs of  $M_{\rm w}=5.5$  in the results shown in Figure 1 we would get four more EQs all in 2022, see [119–122]. From these four EQs, two of them [119,120] were preceded by a SES recorded at ASS on 21 December 2021, i.e., 19 and 26 days before the EQs, respectively. The EQ epicenters lie approximately 140 km away from ASS geoelectric field station inside or close ( $\approx$ 40 km) to the ASS selectivity map (Figure 2 of [123]). The SES amplitude was not indicating that an EQ of  $M \geq 6.0$  was impending and for this reason, the SES on 21 December 2021 was not publicized. As concerns the other two EQs [121,122] with epicentral distances of 120 and 320 km from PIR and KER, respectively, they were not preceded by detectable SES. Hence, we observe that when decreasing the target EQ magnitude, the hit rate also decreases since SES are more easily masked by ambient noise. Of course, this is not a practical problem since only strong ( $M \geq 6.0$ ) EQs are likely dangerous for inflicting damage to human constructions and fatalities.

We now turn to the importance of the continuation of the experimentation with the VAN telemetric network. We already discussed that during our study period a very rare bay-like SES was recorded at KER, indicating that the KER geoelectric field station may provide information on the seismicity in southern Greece. Moreover, SES KER2 that preceded the two stronger EQs in Figure 1 indicates that the selectivity map of KER should be augmented by taking into consideration these two new epicenter locations. We should always have in mind that the VAN method is continuously improved as new strong EQs occur and their corresponding SES are identified.

The VAN method is unique [16] in providing information for *M*6 class EQs which cannot be superseded by the more recent EQ prediction methods developed by NTA [39,51]. The latter, which are based on seismological data only, are focused on either *M*7 class or *M*8 and *M*9 class EQs. This is an additional reason for the importance of the VAN telemetric network in Greece since *M*7 class EQs are rare in Greece, see, e.g., the discussion in Section 2.1.

Finally, we note that machine learning methods have been also applied for the automatic detection of SES using data from the VAN telemetric network. The initial attempts were based on deep learning methods[124] while recently long short-term memory autoencoders have been used[125,126]. The results obtained are very promising, and real-time application of these methods is planned for the future.

# 5. Conclusions

The application of the VAN method in Greece during the period 1 January 2022 to 31 August 2025 led to the following main conclusions:

- 1. All strong  $M_w > 5.5$  EQs within the area  $N_{34.5}^{41.5}E_{20.0}^{27.5}$ , see Figure 1, have been preceded by SES reported well before the EQ occurrence (see Table 1);
- 2. The VAN method is statistically significant, leading to a false alarm rate of 4.8%;
- 3. The study of the AUC in the ROC diagrams points to the characterization of the method as outstanding;
- 4. The continuation of experimentation on the VAN method in Greece will improve the accuracy of the related predictions.

**Author Contributions:** Conceptualization, N.V.S., E.S.S., and P.A.V.; methodology, N.V.S., E.S.S., and P.A.V.; software, N.V.S., and E.S.S.; validation, E.S.S.; formal analysis, N.V.S. and P.A.V.; investigation,

N.V.S., E.S.S., and P.A.V.; resources, N.V.S., E.S.S., and P.A.V.; data curation, N.V.S., and E.S.S.; writing—original draft preparation, N.V.S.; writing—review and editing, N.V.S., E.S.S., and P.A.V.; visualization, N.V.S., and E.S.S.; supervision, N.V.S.; project administration, N.V.S. and P.A.V. All authors have read and agreed to the published version of the manuscript.

Funding: This research received no external funding.

Data Availability Statement: Earthquake data come from either the United States National Earthquake Information Center PDE (downloaded from [55]) or the Institute of Geodynamics of the National Observatory of Athens (downloaded from[114]). The last date seismic data were accessed was 31 August 2025. Gnuplot [127] was used for the preparation of the figures. The Generic Mapping Tools (GMT) [128] were used for the construction of the map in Figure 1. The original contributions presented in this study are included in the article. Further inquiries can be directed to the corresponding author.

**Acknowledgments:** We gratefully acknowledge the continuous supervision and technical support of the geoelectrical stations of the VAN telemetric network by Vasilis Dimitropoulos, Spyros Tzigkos and George Lampithianakis.

**Conflicts of Interest:** The authors declare no conflict of interest.

#### **Abbreviations**

The following abbreviations are used in this manuscript:

ASS Assiros geoelectric field station

AUC Area under the curve

ATH Athens
CH Channel
EQ Earthquake
FN False negative
FP False positive

GI-NOA Institute of geodynamics of the national observatory of Athens

GMT Generic mapping tools

GSM Global system for mobile communications

IOA Ioannina geoelectric field stationKER Keratea geoelectric field stationLAM Lamia geoelectric field stationLOU Loutraki geoelectric field station

M magnitude MAR March

ML(ATH) Local magnitude reported by GI-NOA

PAT Patras geoelectric field station PIR Pirgos geoelectric field station

PSPC Pressure stimulated polarization currents

ROC Receiver operating characteristics

SES Seismic electric signals

TN True negative TP True positive

VAN Varotsos, Alexopoulos, and Nomicos

VOL Volos geoelectric field station USGS United States geological survey

# References

- Sobolev, G.A. Application of electric method to the tentative short-term forecast of Kamchatka earthquakes. *Pure Appl. Geophys.* 1975, 113, 229–235. https://doi.org/10.1007/BF01592913.
- Rikitake, T. Current Research in Earthquake Prediction; D. Reidler Publishing Company: Dordrecht, The Netherlands, 1981.

3. Varotsos, P.; Alexopoulos, K.; Nomicos, K.; Lazaridou, M. Earthquake prediction and electric signals. *Nature* **1986**, 322, 120. https://doi.org/10.1038/322120a0.

- 4. Fraser-Smith, A.C.; Bernardi, A.; McGill, P.R.; Ladd, M.E.; Helliwell, R.A.; Villard, O.G. Low-frequency magnetic-field measurements near the epicenter of the Ms-7.1 Loma-Prieta earthquake. *Geophys. Res. Lett.* **1990**, 17, 1465. https://doi.org/10.1029/GL017i009p01465.
- 5. Varotsos, P.; Lazaridou, M. Latest aspects of earthquake prediction in Greece based on Seismic Electric Signals. *Tectonophysics* **1991**, *188*, 321–347. https://doi.org/10.1016/0040-1951(91)90462-2.
- 6. Varotsos, P.; Alexopoulos, K.; Lazaridou-Varotsou, M.; Nagao, T. Earthquake predictions issued in Greece by seismic electric signals since 6 February 1990. *Tectonophysics* **1993**, 224, 269 288. https://doi.org/10.1016/0040-1951(93)90080-4.
- 7. Monastersky, R. Electric Signals may herald earthquakes. Sci. News 1995, 148, 260.
- 8. Igarashi, G.; Saeki, S.; Takahata, N.; Sumikawa, K.; Tasaka, S.; Sasaki, Y.; Takahashi, M.; Sano, Y. Ground-Water Radon Anomaly Before the Kobe Earthquake in Japan. *Science* **1995**, 269, 60–61. https://doi.org/10.1126/science.269.5220.60.
- 9. Uyeda, S. Introduction to the VAN method of earthquake prediction. In *Proceedings of the Critical Review of VAN: Earthquake Prediction from Seismic Electric Signals*; Lighthill, S.J., Ed.; World Scientific, Singapore, 1996; Volume 16, pp. 3–28. https://doi.org/10.1142/9789812815491\_0001.
- 10. Molchan, G.M. Earthquake prediction as a decision-making problem. *Pure Appl. Geophys.* **1997**, 149, 233–247. https://doi.org/10.1007/BF00945169.
- 11. Uyeda, S. VAN Method of Short-term Earthquake Prediction Shows Promise. Eos. Trans. AGU 1998, 79, 573–580.
- 12. Freund, F. Earthquake prediction is worthy of study. EOS Trans. AGU 1999, 80, 230–232.
- 13. Varotsos, P.A.; Sarlis, N.V.; Skordas, E.S. Spatio-Temporal complexity aspects on the interrelation between Seismic Electric Signals and Seismicity. *Pract. Athens Acad.* **2001**, *76*, 294–321. http://physlab.phys.uoa.gr/org/pdf/p3.pdf.
- 14. Varotsos, P.A.; Sarlis, N.V.; Skordas, E.S. Electric Fields that "arrive" before the time derivative of the magnetic field prior to major earthquakes. *Phys. Rev. Lett.* **2003**, *91*, 148501. https://doi.org/10.1103/PhysRevLett.91.148501.
- 15. Ghosh, D.; Deb, A.; Sengupta, R. Anomalous radon emission as precursor of earthquake. *J. Appl. Geophys.* **2009**, *69*, 67–81. https://doi.org/10.1016/j.jappgeo.2009.06.001.
- 16. Uyeda, S.; Nagao, T.; Kamogawa, M. Short-term earthquake prediction: Current status of seismo-electromagnetics. *Tectonophysics* **2009**, 470, 205–213. https://doi.org/10.1016/j.tecto.2008.07.019.
- 17. Hattori, K.; Serita, A.; Gotoh, K.; Yoshino, C.; Harada, M.; Isezaki, N.; Hayakawa, M. ULF geomagnetic anomaly associated with 2000 Izu Islands earthquake swarm, Japan. *Phys. Chem. Earth Parts A/B/C* **2004**, 29, 425–435. https://doi.org/https://doi.org/10.1016/j.pce.2003.11.014.
- 18. Tramutoli, V.; Cuomo, V.; Filizzola, C.; Pergola, N.; Pietrapertosa, C. Assessing the potential of thermal infrared satellite surveys for monitoring seismically active areas: The case of Kocaeli (İzmit) earthquake, 17 August 1999. *Remote Sens. Environ.* **2005**, 96, 409–426. https://doi.org/10.1016/j.rse.2005.04.006.
- 19. Uyeda, S.; Nagao, T.; Kamogawa, M. Earthquake Precursors and Prediction. In *Encyclopedia of Solid Earth Geophysics*; Springer: Dordrecht, The Netherlands, 2011; pp. 168–178. https://doi.org/10.1007/978-90-481-8702-7\_4.
- 20. Pulinets, S.; Ouzounov, D. Lithosphere—Atmosphere—Ionosphere Coupling (LAIC) model An unified concept for earthquake precursors validation. *J. Asian Earth Sci.* **2011**, *41*, 371–382. https://doi.org/10.1016/j.jseaes.2010.03.005.
- 21. Freund, F. Pre-earthquake signals: Underlying physical processes. *J. Asian Earth Sci.* **2011**, *41*, 383–400. https://doi.org/10.1016/j.jseaes.2010.03.009.
- 22. Lazaridou-Varotsos, M.S. *Earthquake Prediction by Seismic Electric Signals. The Success of the VAN Method Over Thirty Years*; Springer: Berlin/Heidelberg, Germany, 2013. https://doi.org/10.1007/978-3-642-24406-3.
- 23. Xu, G.; Han, P.; Huang, Q.; Hattori, K.; Febriani, F.; Yamaguchi, H. Anomalous behaviors of geomagnetic diurnal variations prior to the 2011 off the Pacific coast of Tohoku earthquake (Mw9.0). *J. Asian Earth Sci.* **2013**, 77, 59–65. https://doi.org/10.1016/j.jseaes.2013.08.011.
- 24. Rozhnoi, A.; Solovieva, M.; Hayakawa, M. VLF/LF signals method for searching of electromagnetic earthquake precursors. In *Earthquake Prediction Studies: Seismo Electromagnetics*; Hayakawa, M., Ed.; TERRAPUB: Tokyo, Japan, 2013; pp. 31–48.
- 25. Chen, C.H.; Wen, S.; Liu, J.Y.; Hattori, K.; Han, P.; Hobara, Y.; Wang, C.H.; Yeh, T.K.; Yen, H.Y. Surface displacements in Japan before the 11 March 2011 M9.0 Tohoku-Oki earthquake. J. Asian Earth Sci. 2014, 80, 165–171. https://doi.org/10.1016/j.jseaes.2013.11.009.
- 26. Orihara, Y.; Kamogawa, M.; Nagao, T. Preseismic Changes of the Level and Temperature of Confined Groundwater related to the 2011 Tohoku Earthquake. *Sci. Rep.* **2014**, *4*, 6907. https://doi.org/10.1038/srep06907.
- 27. Han, P.; Hattori, K.; Xu, G.; Ashida, R.; Chen, C.H.; Febriani, F.; Yamaguchi, H. Further investigations of geomagnetic diurnal variations associated with the 2011 off the Pacific coast of Tohoku earthquake (Mw 9.0). *J. Asian Earth Sci.* 2015, 114, 321–326. https://doi.org/10.1016/j.jseaes.2015.02.022.

28. Han, P.; Hattori, K.; Huang, Q.; Hirooka, S.; Yoshino, C. Spatiotemporal characteristics of the geomagnetic diurnal variation anomalies prior to the 2011 Tohoku earthquake (Mw 9.0) and the possible coupling of multiple pre-earthquake phenomena. *J. Asian Earth Sci.* **2016**, *129*, 13–21. https://doi.org/10.1016/j.jseaes.2016.07.011.

- 29. Hayakawa, T.; Asano, T.; Rozhnoi, A.; Solovieva, M. VLF/LF sounding of ionospheric perturbations and possible association with earthquakes. In *Pre-Earthquake Processes: A Multidisciplinary Approach to Earthquake Prediction Studies*; Ouzounov, D., Pulinets, S., Hattori, K., Taylor, P., Eds.; Geophysical Monograph Series; American Geophysical Union: Hoboken, WA, USA, 2018; pp. 277–304.
- 30. Varotsos, P.A.; Sarlis, N.V.; Skordas, E.S. Phenomena preceding major earthquakes interconnected through a physical model. *Ann. Geophys.* **2019**, *37*, 315–324. https://doi.org/10.5194/angeo-37-315-2019.
- 31. Shen, X.; Zhang, X.; Yuan, S.; Wang, L.; Cao, J.; Huang, J.; Zhu, X.; Piergiorgio, P.; Dai, J. The state-of-the-art of the China Seismo-Electromagnetic Satellite mission. *Sci.-China-Technol. Sci.* 2018, 61, 634–642. https://doi.org/10.1007/s11431-018-9242-0.
- 32. Sarlis, N.V.; Skordas, E.S. Study in Natural Time of Geoelectric Field and Seismicity Changes Preceding the Mw6.8 Earthquake on 25 October 2018 in Greece. *Entropy* **2018**, 20, 882. https://doi.org/10.3390/e20110882.
- 33. Gitis, V.; Derendyaev, A. From monitoring of seismic fields to the automatic forecasting of earthquakes. *Int. J. Web Inf. Syst.* **2019**, 15, 535–549. https://doi.org/10.1108/IJWIS-12-2018-0087.
- 34. Cianchini, G.; De Santis, A.; Di Giovambattista, R.; Abbattista, C.; Amoruso, L.; Campuzano, S.A.; Carbone, M.; Cesaroni, C.; De Santis, A.; Marchetti, D.; et al. Revised Accelerated Moment Release Under Test: Fourteen Worldwide Real Case Studies in 2014–2018 and Simulations. *Pure Appl. Geophys.* 2020, 177, 4057–4087. https://doi.org/10.1007/s00024-020-02461-9.
- 35. Chen, C.H.; Yeh, T.K.; Wen, S.; Meng, G.; Han, P.; Tang, C.C.; Liu, J.Y.; Wang, C.H. Unique Pre-Earthquake Deformation Patterns in the Spatial Domains from GPS in Taiwan. *Remote Sens.* **2020**, *12*, 366. https://doi.org/10.3390/rs12030366.
- 36. Potirakis, S.M.; Schekotov, A.; Contoyiannis, Y.; Balasis, G.; Koulouras, G.E.; Melis, N.S.; Boutsi, A.Z.; Hayakawa, M.; Eftaxias, K.; Nomicos, C. On Possible Electromagnetic Precursors to a Significant Earthquake (Mw = 6.3) Occurred in Lesvos (Greece) on 12 June 2017. *Entropy* **2019**, *21*, 241. https://doi.org/10.3390/e21030241.
- 37. Potirakis, S.M.; Contoyiannis, Y.; Schekotov, A.; Eftaxias, K.; Hayakawa, M. Evidence of critical dynamics in various electromagnetic precursors. *Eur. Phys. J. Spec. Top.* **2021**, 230, 151–177. https://doi.org/10.1140/epjst/e2020-000249-x.
- 38. Varotsos, P.A.; Sarlis, N.V.; Skordas, E.S. Order Parameter and Entropy of Seismicity in Natural Time before Major Earthquakes: Recent Results. *Geosciences* **2022**, *12*, 225. https://doi.org/10.3390/geosciences12060225.
- 39. Varotsos, P.A.; Sarlis, N.V.; Skordas, E.S. *Natural Time Analysis: The New View of Time, Part II. Advances in Disaster Prediction Using Complex Systems*; Springer Nature Switzerland AG: Cham, Switzerland, 2023. https://doi.org/10.1007/978-3-031-26006-3.
- 40. Wibowo, A.; Purnama, S.R.; Pratama, C.; Heliani, L.S.; Sahara, D.P.; Wibowo, S.T. Anomaly detection on displacement rates and deformation pattern features using tree-based algorithm in Japan and Indonesia. *Geod. Geodyn.* **2023**, *14*, 150–162. https://doi.org/10.1016/j.geog.2022.07.003.
- 41. Chi, C.; Li, C.; Han, Y.; Yu, Z.; Li, X.; Zhang, D. Pre-earthquake anomaly extraction from borehole strain data based on machine learning. *Sci. Rep.* **2023**, *13*, 20095. https://doi.org/10.1038/s41598-023-47387-z.
- 42. Ouzounov, D.; Khachikyan, G. Studying the Impact of the Geospace Environment on Solar Lithosphere Coupling and Earthquake Activity. *Remote Sens.* **2024**, *16*, 24. https://doi.org/10.3390/rs16010024.
- 43. Rosca, C.M.; Stancu, A. Earthquake Prediction and Alert System Using IoT Infrastructure and Cloud-Based Environmental Data Analysis. *Appl. Sci.* **2024**, *14*, 10169. https://doi.org/10.3390/app142210169.
- 44. Mukherjee, B.; Shaw, R.L.; Sharma, M.L.; Sain, K. Earthquake prediction using machine learning perspectives in Himalayan seismic belt and its surroundings. *J. Asian Earth Sci.* **2025**, 293, 106764. https://doi.org/10.1016/j.jseaes.2025.106764.
- 45. Neha; Chuang, R.Y.; Nishimura, T.; Lee, Z.; Gao, J.C. Balancing of geodetic and seismic moment rates and its implications for probabilistic seismic hazard analysis in Taiwan. *Earth Planets Space* **2025**, 77, 125. https://doi.org/10.1186/s40623-025-02247-0.
- 46. Graciosa, J.C.; Corbi, F.; Capitanio, F.A. Uncovering Deformation Prior to Analogue Megathrust Earthquakes With Explainable Artificial Intelligence. *Geophys. Res. Lett.* **2025**, 52, e2024GL114428. https://doi.org/10.1029/2024GL114428.
- 47. Varotsos, P.; Alexopoulos, K.; Nomicos, K. Seismic Electric Currents. Pract. Athens Acad. 1981, 56, 277–286.
- 48. Varotsos, P.; Alexopoulos, K.; Nomicos, K. Seven-hour precursors to earthquakes determined from telluric currents. *Pract. Athens Acad.* **1981**, *56*, 417–433.
- 49. Varotsos, P.; Alexopoulos, K.; Lazaridou, M. Latest aspects of earthquake prediction in Greece based on Seismic Electric Signals, II. *Tectonophysics* **1993**, 224, 1–37. https://doi.org/10.1016/0040-1951(93)90055-O.
- 50. Varotsos, P. The Physics of Seismic Electric Signals; TERRAPUB: Tokyo, Japan, 2005; p. 338.
- 51. Varotsos, P.A.; Sarlis, N.V.; Skordas, E.S. *Natural Time Analysis: The New View of Time. Precursory Seismic Electric Signals, Earthquakes and Other Complex Time-Series*; Springer: Berlin/Heidelberg, Germany, 2011. https://doi.org/10.1007/978-3-642-16449-1.
- 52. Varotsos, P.; Alexopoulos, K. *Thermodynamics of Point Defects and Their Relation with Bulk Properties*; North Holland: Amsterdam, The Netherlands, 1986.

53. Varotsos, P.; Sarlis, N.; Lazaridou, M.; Kapiris, P. Transmission of stress induced electric signals in dielectric media. *J. Appl. Phys.* **1998**, *83*, 60–70. https://doi.org/10.1063/1.366702.

- 54. Sarlis, N.; Lazaridou, M.; Kapiris, P.; Varotsos, P. Numerical Model of the Selectivity Effect and ΔV/L criterion. *Geophys. Res. Lett.* **1999**, *26*, 3245–3248. https://doi.org/10.1029/1998GL005265.
- 55. United States Geological Survey, Earthquake Hazards Program. Search Earthquake Catalog. Available online: https://earthquake.usgs.gov/earthquakes/search/ (accessed on 31 August 2025).
- 56. Kanamori, H. Quantification of Earthquakes. *Nature* **1978**, 271, 411–414. https://doi.org/10.1038/271411a0.
- 57. Hanks, T.C.; Kanamori, H. A moment magnitude scale. *J. Geophys. Res.* **1979**, *84*, 2348–2350. https://doi.org/10.1029/JB084iB0 5p02348.
- 58. United States Geological Survey, Earthquake Hazards Program. M6.9—Southern Greece, Greece. Available online: https://earthquake.usgs.gov/earthquakes/eventpage/usp000fyw4/executive (accessed on 31 August 2025).
- 59. Sarlis, N.V.; Skordas, E.S.; Lazaridou, M.S.; Varotsos, P.A. Investigation of seismicity after the initiation of a Seismic Electric Signal activity until the main shock. *Proc. Jpn. Acad. Ser. B Phys. Biol. Sci.* **2008**, *84*, 331–343. https://doi.org/10.2183/pjab.84.331.
- 60. Uyeda, S.; Kamogawa, M. The Prediction of Two Large Earthquakes in Greece. *Eos Trans. AGU* **2008**, *89*, 363. https://doi.org/10.1029/2008EO390002.
- 61. Uyeda, S.; Kamogawa, M. Comment on 'The Prediction of Two Large Earthquakes in Greece'. *Eos. Trans. AGU* **2010**, *91*, 163. https://doi.org/10.1029/2010EO180004.
- 62. USGS. 2010. See the United States Geological Survey (USGS) Earthquake Search Web Page for the Relevant Seismic Catalogues. Available online: http://neic.usgs.gov/neis/epic/epic.html (accessed on 31 August 2025).
- 63. United States Geological Survey, Earthquake Hazards Program. M7.0—26 km SW of Lixoúri, Greece. Available online: https://earthquake.usgs.gov/earthquakes/eventpage/usp0001sa1/executive (accessed on 31 August 2025).
- 64. Sarlis, N.V. Statistical Significance of Earth's Electric and Magnetic Field Variations Preceding Earthquakes in Greece and Japan Revisited. *Entropy* **2018**, *20*, 561. https://doi.org/10.3390/e20080561.
- 65. Varotsos, P.; Sarlis, N.; Lazaridou, M. Reply to "Rebuttal to Reply by Varotsos and Lazaridou: Towards plainly successful prediction," by Paul W. Burton. *Geophys. Res. Lett.* **1996**, 23, 1389–1390. https://doi.org/10.1029/96GL01259.
- 66. Varotsos, P.A.; Sarlis, N.V.; Skordas, E.S.; Lazaridou-Varotsos, M.S. Identifying the occurrence time of an impending mainshock: A very recent case. *arXiv* **2025**, arXiv1908.00279.
- 67. Sarlis, N.V.; Skordas, E.S.; Varotsos, P.A. Geoelectric field and seismicity changes preceding the 2018 Mw6.8 earthquake and the subsequent activity in Greece. *arXiv* 2024, arXiv:901.06658.
- 68. United States Geological Survey, Earthquake Hazards Program. M 4.9—4 km SSW of Níkiti, Greece. Available online: https://earthquake.usgs.gov/earthquakes/eventpage/us6000jm7j/executive (accessed on 31 August 2025).
- 69. United States Geological Survey, Earthquake Hazards Program. M5.3—56 km SW of Palaióchora, Greece. Available online: https://earthquake.usgs.gov/earthquakes/eventpage/us7000n0l7/executive (accessed on 31 August 2025).
- 70. Uyeda, S.; Kamogawa, M.; Tanaka, H. Analysis of electrical activity and seismicity in the natural time domain for the volcanic-seismic swarm activity in 2000 in the Izu Island region, Japan. *J. Geophys. Res. Solid Earth* **2009**, *114*, B02310. https://doi.org/10.1029/2007JB005332.
- 71. Uyeda, S.; Nagao, T.; Orihara, Y.; Yamaguchi, T.; Takahashi, I. Geoelectric potential changes: Possible precursors to earthquakes in Japan. *Proc. Natl. Acad. Sci. USA* **2000**, *97*, 4561–4566. https://doi.org/10.1073/pnas.97.9.4561.
- 72. Uyeda, S.; Hayakawa, M.; Nagao, T.; Molchanov, O.; Hattori, K.; Orihara, Y.; Gotoh, K.; Akinaga, Y.; Tanaka, H. Electric and magnetic phenomena observed before the volcano-seismic activity in 2000 in the Izu Island Region, Japan. *Proc. Natl. Acad. Sci. USA* 2002, 99, 7352–7355. https://doi.org/10.1073/pnas.072208499.
- 73. Orihara, Y.; Kamogawa, M.; Nagao, T.; Uyeda, S. Preseismic anomalous telluric current signals observed in Kozu-shima Island, Japan. *Proc. Natl. Acad. Sci. USA* **2012**, *109*, 19125–19128. https://doi.org/10.1073/pnas.1215669109.
- 74. Zlotnicki, J.; Kossobokov, V.; Le Mouël, J.L. Frequency spectral properties of an ULF electromagnetic signal around the 21 July 1995, M=5.7, Yong Deng (China) earthquake. *Tectonophysics* **2001**, 334, 259 270. https://doi.org/10.1016/S0040-1951(00)00222-5.
- 75. Fan, Y.Y.; Du, X.B.; Zlotnicki, J.; Tan, D.C.; An, Z.H.; Chen, J.Y.; Zheng, G.L.; Liu, J.; Xie, T. The Electromagnetic Phenomena Before the Ms8.0 Wenchuan Earthquake. *Chinese J. Geophys.* **2010**, *53*, 997–1010. https://doi.org/10.1002/cjg2.1570.
- 76. Huang, Q. Retrospective investigation of geophysical data possibly associated with the Ms8.0 Wenchuan earthquake in Sichuan, China . *J. Asian Earth Sci.* **2011**, *41*, 421 427. https://doi.org/10.1016/j.jseaes.2010.05.014.
- 77. Ramírez-Rojas, A.; Flores-Márquez, E.L.; Guzmán-Vargas, L.; Gálvez-Coyt, G.; Telesca, L.; Angulo-Brown, F. Statistical features of seismoelectric signals prior to M7.4 Guerrero-Oaxaca earthquake (México). *Nat. Hazards Earth Syst. Sci.* **2008**, *8*, 1001–1007. https://doi.org/10.5194/nhess-8-1001-2008.
- 78. Ramírez-Rojas, A.; Telesca, L.; Angulo-Brown, F. Entropy of geoelectrical time series in the natural time domain. *Nat. Hazards Earth Syst. Sci.* **2011**, *11*, 219–225. https://doi.org/10.5194/nhess-11-219-2011.

79. Papadopoulou, K.; Skordas, E.; Zlotnicki, J.; Nagao, T.; Rybin, A. Study of Geo-Electric Data Collected by the Joint EMSEV-Bishkek RS-RAS Cooperation: Possible Earthquake Precursors. *Entropy* **2018**, 20, 614. https://doi.org/10.3390/e20080614.

- 80. Sarlis, N.; Varotsos, P. Magnetic field near the outcrop of an almost horizontal conductive sheet. *J. Geodyn.* **2002**, *33*, 463–476. https://doi.org/10.1016/S0264-3707(02)00008-X.
- 81. Uyeda, S.; Al-Damegh, E.; Dologlou, E.; Nagao, T. Some relationship between VAN seismic electric signals (SES) and earthquake parameters. *Tectonophysics* **1999**, 304, 41–55. https://doi.org/10.1016/S0040-1951(98)00301-1.
- 82. Feller, W. An Introduction to Probability Theory and Its Applications, Vol. II; Wiley: New York, NY, USA, 1971.
- 83. Lesche, B. Instabilities of Renyi entropies. J. Stat. Phys. 1982, 27, 419. https://doi.org/10.1007/BF01008947.
- 84. Lesche, B. Renyi entropies and observables. Phys. Rev. E 2004, 70, 017102. https://doi.org/10.1103/PhysRevE.70.017102.
- 85. Varotsos, P.; Alexopoulos, K. Physical Properties of the variations of the electric field of the Earth preceding earthquakes, I. *Tectonophysics* **1984**, *110*, 73–98. https://doi.org/10.1016/0040-1951(84)90059-3.
- 86. Varotsos, P.; Alexopoulos, K. Physical Properties of the variations of the electric field of the Earth preceding earthquakes, II. *Tectonophysics* **1984**, *110*, 99–125. https://doi.org/10.1016/0040-1951(84)90060-X.
- 87. Nomicos, K.; Chatzidiakos, P. A telemetric system for measuring electrotelluric variations in Greece and its application to Earthquake prediction. *Tectonophysics* **1993**, 224, 39–46. https://doi.org/10.1016/0040-1951(93)90056-P.
- 88. Nomicos, K.; Makris, J.; Kefalas, M. The telemetric system of VAN group. In *The Critical Review of VAN: Earthquake Prediction from Seismic Electric Signals*; Lighthill, S.J., Ed.; World Scientific, Singapore, 1996; pp. 77–88. https://doi.org/10.1142/9789812815491\_0003.
- 89. Fawcett, T. An introduction to ROC analysis. Pattern Recogn. Lett. 2006, 27, 861–874. https://doi.org/10.1016/j.patrec.2005.10.010.
- 90. Mason, S.J.; Graham, N.E. Areas beneath the relative operating characteristics (ROC) and relative operating levels (ROL) curves: Statistical significance and interpretation. *Q. J. R. Meteor. Soc.* **2002**, *128*, 2145–2166. https://doi.org/10.1256/003590002320603584.
- 91. Mann, H.B.; Whitney, D.R. On a Test of Whether one of Two Random Variables is Stochastically Larger than the Other. *Ann. Math. Statist.* **1947**, *18*, 50–60. https://doi.org/10.1214/aoms/1177730491.
- 92. Sarlis, N.V.; Christopoulos, S.R.G. Visualization of the significance of Receiver Operating Characteristics based on confidence ellipses. *Comput. Phys. Commun.* **2014**, *185*, 1172–1176. https://doi.org/10.1016/j.cpc.2013.12.009.
- 93. Christopoulos, S.R.G.; Tsagiannis, G.I.; Papadopoulou, K.A.; Sarlis, N.V. VISROC 2.0: Updated Software for the Visualization of the significance of Receiver Operating Characteristics based on confidence ellipses. *Comput. Phys. Commun.* **2022**, 280, 108492. https://doi.org/10.1016/j.cpc.2022.108492.
- 94. Steyerberg, E.W.; Vickers, A.J.; Cook, N.R.; Gerds, T.; Gonen, M.; Obuchowski, N.; Pencina, M.J.; Kattan, M.W. Assessing the Performance of Prediction Models A Framework for Traditional and Novel Measures. *Epidemiology* **2010**, 21, 128–138. https://doi.org/10.1097/EDE.0b013e3181c30fb2.
- 95. Mandrekar, J.N. Receiver Operating Characteristic Curve in Diagnostic Test Assessment. *J. Thorac. Oncol.* **2010**, *5*, 1315–1316. https://doi.org/10.1097/JTO.0b013e3181ec173d.
- 96. Hosmer, D.W.; Lemeshow, S. Applied Logistic Regression; John Wiley & Sons, Ltd.: New York, NY, USA, 2000. https://doi.org/10.102/0471722146.
- 97. Fitterman, D.V. Theory of electrokinetic and magnetic anomalies associated with dilatant regions in a layered Earth. *J. Geophys. Res. Solid Earth* **1978**, *83*, 5923–5928. https://doi.org/10.1029/JB083iB12p05923.
- 98. Fitterman, D.V. Calculation of self-potential anomalies near vertical contacts. *Geophys* **1979**, 44, 195–205. https://doi.org/10.119 0/1.1440961.
- 99. Gershenzon, N.; Gokhberg, M. On the origin of electrotelluric disturbances prior to an earthquake in Kalamata, Greece. *Tectonophysics* **1993**, 224, 169–174. https://doi.org/10.1016/0040-1951(93)90069-V.
- 100. Ishido, T.; Mizutani, H. Experimental and theoretical basis of electrokinetic phenomena in rock-water systems and its applications to geophysics. *J. Geophys. Res. Solid Earth* **1981**, *86*, 1763–1775. https://doi.org/10.1029/JB086iB03p01763.
- 101. Jouniaux, L.; Pozzi, J.P. Streaming potential and permeability of saturated sandstones under triaxial stress: Consequences for electrotelluric anomalies prior to earthquakes. *J. Geophys. Res. Solid Earth* **1995**, *100*, 10197–10209. https://doi.org/10.1029/95JB0 0069.
- 102. Jouniaux, L.; Pozzi, J.P. Laboratory measurements anomalous 0.1–0.5 Hz streaming potential under geochemical changes: Implications for electrotelluric precursors to earthquakes. *J. Geophys. Res. Solid Earth* **1997**, 102, 15335–15343. https://doi.org/10.1029/97JB00955.
- 103. Mizutani, H.; Ishido, T. A new interpretation of magnetic field variation associated with Matsushiro earthquakes. *J. Geomagn. Geoelectr.* **1976**, *28*, 179–188. https://doi.org/10.5636/jgg.28.179.
- 104. Mizutani, H.; Ishido, T.; Yokokura, T.; Ohnishi, S. Electrokinetic phenomena associated with earthquakes. *Geophys. Res. Lett.* **1976**, 3, 365–368. https://doi.org/10.1029/GL003i007p00365.
- 105. Morgan, D. A model for the explanation of SES-generation based on electrokinetic effect. In Proceedings of the International Conference on Measurements and Theoretical Models of the Earth's Field Variations Related to Earthquakes, Athens, Greece, 6–8 February 1990; p. 57.

106. Morgan, F.D. Electrodynamics of the earthquake source. In Proceedings of the Eos, Transactions, American Geophysical Union Supply—AGU 1995 Fall Meeting, San Francisco, CA, USA, 11–15 December 1995; F173.

- 107. Sornette, A.; Sornette, D. Earthquake rupture as a critical point: Consequences for telluric precursors. *Tectonophysics* **1990**, 179, 327–334. https://doi.org/10.1016/0040-1951(90)90298-M.
- 108. Slifkin, L. Seismic electric signals displacement of charged dislocations. *Tectonophysics* **1993**, 224, 149–152. https://doi.org/10.101 6/0040-1951(93)90066-S.
- 109. Slifkin, L. A dislocation model for seismic electric signals. In *Critical Review of VAN: Earthquake Prediction from Seismic Electric Signals*; Lighthill, S.J., Ed.; World Scientific, Singapore, 1996; pp. 97–104. https://doi.org/10.1142/9789812815491\_0005.
- 110. Lazarus, D. Short term earthquake prediction in Greece by Seismic Electric Signals. In *Proceedings of the Critical Review of VAN: Earthquake Prediction from Seismic Electric Signals*; Lighthill, S.J., Ed.; World Scientific, Singapore, 1996; pp. 91–96. https://doi.org/10.1142/9789812815491\_0004.
- 111. Varotsos, P.; Alexopoulos, K. Physical properties of the variations in the electric field of the earth preceding earthquakes, III. *Tectonophysics* **1987**, *136*, 335–339. https://doi.org/10.1016/0040-1951(87)90033-3.
- 112. United States Geological Survey, Earthquake Hazards Program. M6.0—1 km ENE of Paralía Vérgas, Greece. Available online: https://earthquake.usgs.gov/earthquakes/eventpage/usp0002y1v/executive (accessed on 31 August 2025).
- 113. Anagnostopolous, S.A.; Rinaldis, D.; Lekidis, V.A.; Margaris, V.N.; Theodulidis, N.P. The Kalamata, Greece, Earthquake of 13 September 1986. *Earthq. Spectra* **1987**, *3*, 365–402. https://doi.org/10.1193/1.1585434.
- 114. National Observatory of Athens, Institute of Geodynamics. Earthquake Catalogues. Available online: https://www.gein.noa.gr/en/services-products/recent-seismicity/ (accessed on 31 August 2025).
- 115. Varotsos, P.A.; Sarlis, N.V.; Skordas, E.S.; Christopoulos, S.R.G.; Lazaridou-Varotsos, M.S. Identifying the occurrence time of an impending mainshock: A very recent case. *Earthq. Sci.* **2015**, *28*, 215–222. https://doi.org/10.1007/s11589-015-0122-3.
- 116. Varotsos, P.; Sarlis, N.; Skordas, E. A note on the spatial extent of the Volos SES sensitive site. Acta Geophys. Pol. 2001, 49, 425-435.
- 117. Lazaridou-Varotsos, M.S. Disastrous Athens earthquake, 1999. In *Earthquake Prediction by Seismic Electric Signals: The Success of the VAN Method over Thirty Years*; Springer: Berlin/Heidelberg, Germany, 2013; pp. 155–158. https://doi.org/10.1007/978-3-642-24406-3\_17.
- 118. Varotsos, P.A.; Sarlis, N.V.; Skordas, E.S.; Lazaridou, M.S. Fluctuations, under time reversal, of the natural time and the entropy distinguish similar looking electric signals of different dynamics. *J. Appl. Phys.* **2008**, *103*, 014906. https://doi.org/10.1063/1.28 27363.
- 119. United States Geological Survey, Earthquake Hazards Program. M5.5—5 km NNW of Flórina, Greece. Available online: https://earthquake.usgs.gov/earthquakes/eventpage/us7000gaex/executive (accessed on 31 August 2025).
- 120. United States Geological Survey, Earthquake Hazards Program. M5.5—25 km SSE of Karyes, Greece. Available online: https://earthquake.usgs.gov/earthquakes/eventpage/us7000gcfq/executive (accessed on 31 August 2025).
- 121. United States Geological Survey, Earthquake Hazards Program. M5.5—45 km SW of Lixoúri, Greece. Available online: https://earthquake.usgs.gov/earthquakes/eventpage/us6000ii2v/executive (accessed on 31 August 2025).
- 122. United States Geological Survey, Earthquake Hazards Program. M5.5—Crete, Greece. Available online: https://earthquake.usgs.gov/earthquakes/eventpage/us7000ir86/executive (accessed on 31 August 2025).
- 123. Sarlis, N.V. On the recent seismic activity in North-Eastern Aegean Sea including the  $M_w$  5.8 earthquake on 8 January 2013. *Proc. Jpn. Acad. Ser. B Phys. Biol. Sci.* **2013**, 89, 438–445. https://doi.org/10.2183/pjab.89.438.
- 124. Kanarachos, S.; Christopoulos, S.R.G.; Chroneos, A.; Fitzpatrick, M.E. Detecting anomalies in time series data via a deep learning algorithm combining wavelets, neural networks and Hilbert transform. *Expert Syst. Appl.* **2017**, *85*, 292–304. https://doi.org/10.1016/j.eswa.2017.04.028.
- 125. Xue, J.; Huang, Q.; Wu, S.; Nagao, T. LSTM-Autoencoder Network for the Detection of Seismic Electric Signals. *IEEE Trans. Geosci. Remote. Sens.* **2022**, *60*, 5917012. https://doi.org/10.1109/TGRS.2022.3183389.
- 126. Xue, J.; Wu, S.; Huang, Q.; Zhao, L.; Sarlis, N.V.; Varotsos, P.A. RASE: A Real-Time Automatic Search Engine for Anomalous Seismic Electric Signals in Geoelectric Data. *IEEE Trans. Geosci. Remote Sens.* 2023, 61, 5905911. https://doi.org/10.1109/TGRS.2023.3260202.
- 127. Williams, T.; Kelley, C. Gnuplot 4.6: An Interactive Plotting Program. 2014. Available online: http://www.gnuplot.info (accessed on 28 February 2014).
- 128. Wessel, P.; Luis, J.F.; Uieda, L.; Scharroo, R.; Wobbe, F.; Smith, W.H.F.; Tian, D. The Generic Mapping Tools Version 6. *Geochem. Geophys. Geosystems* **2019**, 20, 5556–5564. https://doi.org/10.1029/2019GC008515.

**Disclaimer/Publisher's Note:** The statements, opinions and data contained in all publications are solely those of the individual author(s) and contributor(s) and not of MDPI and/or the editor(s). MDPI and/or the editor(s) disclaim responsibility for any injury to people or property resulting from any ideas, methods, instructions or products referred to in the content.